Two-photon widths of the $\chi_{c0,2}$ states and helicity analysis for $\chi_{c2} \to \gamma\gamma$

M. Ablikim,[1] M. N. Achasov,[5] D. J. Ambrose,[40] F. F. An,[1] Q. An,[41] Z. H. An,[1] J. Z. Bai,[1] Y. Ban,[27] J. Becker,[2] N. Berger,[1] M. Bertani,[18] J. M. Bian,[39] E. Boger,[20,*] O. Bondarenko,[21] I. Boyko,[20] R. A. Briere,[3] V. Bytev,[20] X. Cai,[1] A. Calcaterra,[18] G. F. Cao,[1] J. F. Chang,[1] G. Chelkov,[20,*] G. Chen,[1] H. S. Chen,[1] J. C. Chen,[1] M. L. Chen,[1] S. J. Chen,[25] Y. Chen,[1] Y. B. Chen,[1] H. P. Cheng,[14] Y. P. Chu,[1] D. Cronin-Hennessy,[39] H. L. Dai,[1] J. P. Dai,[1] D. Dedovich,[20] Z. Y. Deng,[1] A. Denig,[19] I. Denysenko,[20,†] M. Destefanis,[44] W. M. Ding,[29] Y. Ding,[23] L. Y. Dong,[1] M. Y. Dong,[1] S. X. Du,[47] J. Fang,[1] S. S. Fang,[1] L. Fava,[44,‡] F. Feldbauer,[2] C. Q. Feng,[41] R. B. Ferroli,[18] C. D. Fu,[1] J. L. Fu,[25] Y. Gao,[36] C. Geng,[41] K. Goetzen,[7] W. X. Gong,[1] W. Gradl,[19] M. Greco,[44] M. H. Gu,[1] Y. T. Gu,[9] Y. H. Guan,[6] A. Q. Guo,[26] L. B. Guo,[24] Y. P. Guo,[26] Y. L. Han,[1] X. Q. Hao,[1] F. A. Harris,[38] K. L. He,[1] M. He,[1] Z. Y. He,[26] T. Held,[2] Y. K. Heng,[1] Z. L. Hou,[1] H. M. Hu,[1] J. F. Hu,[6] T. Hu,[1] B. Huang,[1] G. M. Huang,[15] J. S. Huang,[12] X. T. Huang,[29] Y. P. Huang,[1] T. Hussain,[43] C. S. Ji,[41] Q. Ji,[1] X. B. Ji,[1] X. L. Ji,[1] L. K. Jia,[1] L. L. Jiang,[1] X. S. Jiang,[1] J. B. Jiao,[29] Z. Jiao,[14] D. P. Jin,[1] S. Jin,[1] F. F. Jing,[36] N. Kalantar-Nayestanaki,[21] M. Kavatsyuk,[21] W. Kuehn,[37] W. Lai,[1] J. S. Lange,[37] J. K. C. Leung,[35] C. H. Li,[1] Cheng Li,[41] Cui Li,[41] D. M. Li,[47] F. Li,[1] G. Li,[1] H. B. Li,[1] J. C. Li,[1] K. Li,[10] Lei Li,[1] N. B. Li,[24] Q. J. Li,[1] S. L. Li,[1] W. D. Li,[1] W. G. Li,[1] X. L. Li,[29] X. N. Li,[1] X. Q. Li,[26] X. R. Li,[28] Z. B. Li,[33] H. Liang,[41] Y. F. Liang,[31] Y. T. Liang,[37] G. R. Liao,[36] X. T. Liao,[1] B. J. Liu,[34] B. J. Liu,[1] C. L. Liu,[3] C. X. Liu,[1] C. Y. Liu,[1] F. H. Liu,[30] Fang Liu,[1] Feng Liu,[15] H. Liu,[1] H. B. Liu,[6] H. H. Liu,[13] H. M. Liu,[1] H. W. Liu,[1] J. P. Liu,[45] K. Y. Liu,[23] Kai Liu,[6] Kun Liu,[27] P. L. Liu,[29] S. B. Liu,[41] X. Liu,[22] X. H. Liu,[1] Y. Liu,[1] Y. B. Liu,[26] Z. A. Liu,[1] Zhiqiang Liu,[1] Zhiqing Liu,[1] H. Loehner,[21] G. R. Lu,[12] H. J. Lu,[14] J. G. Lu,[1] Q. W. Lu,[30] X. R. Lu,[6] Y. P. Lu,[1] C. L. Luo,[24] M. X. Luo,[46] T. Luo,[38] X. L. Luo,[1] M. Lv,[1] C. L. Ma,[6] F. C. Ma,[23] H. L. Ma,[1] Q. M. Ma,[1] S. Ma,[1] T. Ma,[1] X. Y. Ma,[1] Y. Ma,[11] F. E. Maas,[11] M. Maggiora,[44] Q. A. Malik,[43] H. Mao,[1] Y. J. Mao,[27] Z. P. Mao,[1] J. G. Messchendorp,[21] J. Min,[1] T. J. Min,[1] R. E. Mitchell,[17] X. H. Mo,[1] C. Morales Morales,[11] C. Motzko,[2] N. Yu. Muchnoi,[5] Y. Nefedov,[20] C. Nicholson,[6] I. B. Nikolaev,[5] Z. Ning,[1] S. L. Olsen,[28] Q. Ouyang,[1] S. Pacetti,[18,§] J. W. Park,[28] M. Pelizaeus,[38] K. Peters,[7] J. L. Ping,[24] R. G. Ping,[1] R. Poling,[39] E. Prencipe,[19] C. S. J. Pun,[35] C. S. Qian,[1] C. F. Qiao,[6] X. S. Qin,[1] Y. Qin,[27] Z. H. Qin,[1] J. F. Qiu,[1] K. H. Rashid,[43] G. Rong,[1] X. D. Ruan,[9] A. Sarantsev,[20,∥] J. Schulze,[2] M. Shao,[41] C. P. Shen,[38,¶] X. Y. Shen,[1] H. Y. Sheng,[1] M. R. Shepherd,[17] X. Y. Song,[1] S. Spataro,[44] B. Spruck,[37] D. H. Sun,[1] G. X. Sun,[1] J. F. Sun,[12] S. S. Sun,[1] X. D. Sun,[1] Y. J. Sun,[41] Y. Z. Sun,[1] Z. J. Sun,[1] Z. T. Sun,[41] C. J. Tang,[31] X. Tang,[1] E. H. Thorndike,[40] H. L. Tian,[1] D. Toth,[39] M. Ullrich,[37] G. S. Varner,[38] B. Wang,[9] B. Q. Wang,[27] K. Wang,[1] L. L. Wang,[4] L. S. Wang,[4] M. Wang,[1] P. Wang,[29] P. L. Wang,[1] Q. Wang,[1] Q. J. Wang,[1] S. G. Wang,[27] X. F. Wang,[12] X. L. Wang,[41] Y. D. Wang,[41] Y. F. Wang,[1] Y. Q. Wang,[29] Z. Wang,[1] Z. G. Wang,[1] Z. Y. Wang,[1] D. H. Wei,[8] P. Weidenkaff,[19] Q. G. Wen,[41] S. P. Wen,[1] M. Werner,[37] U. Wiedner,[2] L. H. Wu,[1] N. Wu,[1] S. X. Wu,[41] W. Wu,[26] Z. Wu,[1] L. G. Xia,[36] Z. J. Xiao,[24] Y. G. Xie,[1] Q. L. Xiu,[1] G. F. Xu,[1] G. M. Xu,[27] H. Xu,[1] Q. J. Xu,[10] X. P. Xu,[32] Y. Xu,[26] Z. R. Xu,[41] F. Xue,[15] Z. Xue,[1] L. Yan,[41] W. B. Yan,[41] Y. H. Yan,[16] H. X. Yang,[1] T. Yang,[9] Y. Yang,[15] Y. X. Yang,[8] H. Ye,[1] M. Ye,[1] M. H. Ye,[1] B. X. Yu,[1] C. X. Yu,[26] J. S. Yu,[22] S. P. Yu,[29] C. Z. Yuan,[1] W. L. Yuan,[24] Y. Yuan,[1] A. A. Zafar,[43] A. Zallo,[18] Y. Zeng,[16] B. X. Zhang,[1] B. Y. Zhang,[1] C. C. Zhang,[1] D. H. Zhang,[1] H. H. Zhang,[33] H. Y. Zhang,[1] J. Zhang,[24] J. G. Zhang,[12] J. Q. Zhang,[1] J. W. Zhang,[1] J. Y. Zhang,[1] J. Z. Zhang,[1] L. Zhang,[25] S. H. Zhang,[1] T. R. Zhang,[24] X. J. Zhang,[1] X. Y. Zhang,[29] Y. Zhang,[1] Y. H. Zhang,[1] Y. S. Zhang,[9] Z. P. Zhang,[41] Z. Y. Zhang,[45] G. Zhao,[1] H. S. Zhao,[1] J. W. Zhao,[1] K. X. Zhao,[24] Lei Zhao,[41] Ling Zhao,[1] M. G. Zhao,[26] Q. Zhao,[1] S. J. Zhao,[47] T. C. Zhao,[1] X. H. Zhao,[25] Y. B. Zhao,[1] Z. G. Zhao,[41] A. Zhemchugov,[20,*] B. Zheng,[42] J. P. Zheng,[1] Y. H. Zheng,[6] Z. P. Zheng,[1] B. Zhong,[1] J. Zhong,[2] L. Zhou,[1] X. K. Zhou,[6] X. R. Zhou,[41] C. Zhu,[1] K. Zhu,[1] K. J. Zhu,[1] S. H. Zhu,[1] X. L. Zhu,[36] X. W. Zhu,[1] Y. M. Zhu,[26] Y. S. Zhu,[1] Z. A. Zhu,[1] J. Zhuang,[1] B. S. Zou,[1] J. H. Zou,[1] and J. X. Zuo,[1]

(BESIII Collaboration)

[1]*Institute of High Energy Physics, Beijing 100049, People's Republic of China*
[2]*Bochum Ruhr-University, 44780 Bochum, Germany*
[3]*Carnegie Mellon University, Pittsburgh, Pennsylvania 15213, USA*
[4]*China Center of Advanced Science Technology, Beijing 100190, People's Republic of China*
[5]*G. I. Budker Institute of Nuclear Physics SB RAS (BINP), Novosibirsk 630090, Russia*
[6]*Graduate University of Chinese Academy of Sciences, Beijing 100049, People's Republic of China*
[7]*GSI Helmholtzcentre for Heavy Ion Research GmbH, D-64291 Darmstadt, Germany*
[8]*Guangxi Normal University, Guilin 541004, People's Republic of China*
[9]*GuangXi University, Nanning 530004, People's Republic of China*
[10]*Hangzhou Normal University, Hangzhou 310036, People's Republic of China*
[11]*Helmholtz Institute Mainz, J. J. Becherweg 45, D55099 Mainz, Germany*

^{12}*Henan Normal University, Xinxiang 453007, People's Republic of China*

^{13}*Henan University of Science Technology, Luoyang 471003, People's Republic of China*

^{14}*Huangshan College, Huangshan 245000, People's Republic of China*

^{15}*Huazhong Normal University, Wuhan 430079, People's Republic of China*

^{16}*Hunan University, Changsha 410082 People's Republic of China*

^{17}*Indiana University, Bloomington, Indiana 47405, USA*

^{18}*INFN Laboratori Nazionalidi Frascati, Frascati, Italy*

^{19}*Johannes Gutenberg University of Mainz, Johann-Joachim-Becher-Weg 45, 55099 Mainz, Germany*

^{20}*Joint Institute for Nuclear Research, 141980 Dubna, Russia*

^{21}*KVI/University of Groningen, 9747 AA Groningen, The Netherlands*

^{22}*Lanzhou University, Lanzhou 730000, People's Republic of China*

^{23}*Liaoning University, Shenyang 110036, People's Republic of China*

^{24}*Nanjing Normal University, Nanjing 210046, People's Republic of China*

^{25}*Nanjing University, Nanjing 210093, People's Republic of China*

^{26}*Nankai University, Tianjin 300071, People's Republic of China*

^{27}*Peking University, Beijing 100871, People's Republic of China*

^{28}*Seoul National University, Seoul,151-747 Korea*

^{29}*Shandong University, Jinan 250100, People's Republic of China*

^{30}*Shanxi University, Taiyuan 030006, People's Republic of China*

^{31}*Sichuan University, Chengdu 610064, People's Republic of China*

^{32}*Soochow University, Suzhou 215006, China*

^{33}*SunYat-Sen University, Guangzhou 510275, People's Republic of China*

^{34}*The Chinese University of Hong Kong, Shatin, New Territories, Hong Kong*

^{35}*The University of Hong Kong, Pokfulam, Hong Kong*

^{36}*Tsinghua University, Beijing 100084, People's Republic of China*

^{37}*Universitaet Giessen, 35392 Giessen, Germany*

^{38}*University of Hawaii, Honolulu, Hawaii 96822, USA*

^{39}*University of Minnesota, Minneapolis, MN 55455, USA*

^{40}*University of Rochester, Rochester, New York 14627, USA*

^{41}*University of Science Technology of China, Hefei 230026, People's Republic of China*

^{42}*University of South China, Hengyang 421001, People's Republic of China*

^{43}*University of the Punjab, Lahore-54590, Pakistan*

^{44}*University of Turin INFN, Turin, Italy*

^{45}*Wuhan University, Wuhan 430072, People's Republic of China*

^{46}*Zhejiang University, Hangzhou 310027, People's Republic of China*

^{47}*Zhengzhou University, Zhengzhou 450001, People's Republic of China*

Based on a data sample of 106×10^6 ψ' events collected with the BESIII detector, the decays $\psi' \rightarrow \gamma\chi_{c0,2}$, $\chi_{c0,2} \rightarrow \gamma\gamma$ are studied to determine the two-photon widths of the $\chi_{c0,2}$ states. The two-photon decay branching fractions are determined to be $\mathcal{B}(\chi_{c0} \rightarrow \gamma\gamma) = (2.24 \pm 0.19 \pm 0.12 \pm 0.08) \times 10^{-4}$ and $\mathcal{B}(\chi_{c2} \rightarrow \gamma\gamma) = (3.21 \pm 0.18 \pm 0.17 \pm 0.13) \times 10^{-4}$. From these, the two-photon widths are determined to be $\Gamma_{\gamma\gamma}(\chi_{c0}) = (2.33 \pm 0.20 \pm 0.13 \pm 0.17)$ keV, $\Gamma_{\gamma\gamma}(\chi_{c2}) = (0.63 \pm 0.04 \pm 0.04 \pm 0.04)$ keV, and $\mathcal{R} = \Gamma_{\gamma\gamma}(\chi_{c2})/\Gamma_{\gamma\gamma}(\chi_{c0}) = 0.271 \pm 0.029 \pm 0.013 \pm 0.027$, where the uncertainties are statistical, systematic, and those from the PDG $\mathcal{B}(\psi' \rightarrow \gamma\chi_{c0,2})$ and $\Gamma(\chi_{c0,2})$ errors, respectively. The ratio of the two-photon widths for helicity $\lambda = 0$ and helicity $\lambda = 2$ components in the decay $\chi_{c2} \rightarrow \gamma\gamma$ is measured for the first time to be $f_{0/2} = \Gamma_{\gamma\gamma}^{\lambda=0}(\chi_{c2})/\Gamma_{\gamma\gamma}^{\lambda=2}(\chi_{c2}) = 0.00 \pm 0.02 \pm 0.02$.

---

*Also at the Moscow Institute of Physics and Technology, Moscow, Russia.

†On leave from the Bogolyubov Institute for Theoretical Physics, Kiev, Ukraine.

‡Present address: University of Piemonte Orientale and INFN, Turin, Italy.

§Currently at INFN and University of Perugia, I-06100 Perugia, Italy.

‖Also at the PNPI, Gatchina, Russia.

¶Currently at Nagoya University, Nagoya, Japan.

I. INTRODUCTION

Charmonium physics is in the boundary domain between perturbative and nonperturbative quantum chromodynamics (QCD). Notably, the two-photon decays of *P*-wave charmonia are helpful for better understanding the nature of interquark forces and decay mechanisms [1]. In particular, the decays of $\chi_{c0,2} \rightarrow \gamma\gamma$ offer the closest parallel between quantum electrodynamics (QED) and QCD, being completely analogous to the decays of the

corresponding triplet states of positronium. In the lowest order, for both positronium and charmonium the ratio of the two-photon decays [2]

$$\mathcal{R}^{(0)}_{th} \equiv \frac{\Gamma(^3P_2 \rightarrow \gamma\gamma)}{\Gamma(^3P_0 \rightarrow \gamma\gamma)} = 4/15 \approx 0.27.$$

Any discrepancy from this simple lowest order prediction can arise due to QCD radiative corrections and relativistic corrections, and the measurement of $\mathcal{R}$ provides useful information on these effects. The decay of $\chi_{c1} \rightarrow \gamma\gamma$ is forbidden by the Landau-Yang theorem [3]. Theoretical predictions on the decay rates are obtained using a non-relativistic approximation [4,5], potential model [6], relativistic quark model [7,8], nonrelativistic QCD factorization framework [9], effective Lagrangian [10], as well as lattice calculations [11]. The predictions for the ratio $\mathcal{R} \equiv \Gamma_{\gamma\gamma}(\chi_{c2})/\Gamma_{\gamma\gamma}(\chi_{c0})$ cover a wide range values between 0.09 and 0.36 [6,8]. Precision measurements of these quantities will guide the development of QCD theory.

The two-photon decay widths of χ_{cJ} have been measured by many experiments [12]. Using the reactions $\psi' \rightarrow \gamma\chi_{cJ}$, the CLEO-c experiment reported results for $\Gamma_{\gamma\gamma}(\chi_{cJ})$ measured in the decay of χ_{cJ} into two photons [13]:

$$\begin{aligned} \Gamma_{\gamma\gamma}(\chi_{c0}) &= (2.36 \pm 0.35 \pm 0.22)\,\text{keV}, \\ \Gamma_{\gamma\gamma}(\chi_{c2}) &= (0.66 \pm 0.07 \pm 0.06)\,\text{keV}, \end{aligned} \quad (1)$$

with uncertainties that are dominated by the statistical errors. BESIII has collected 106×10^6 ψ' events, a data sample that is about 4 times of that of CLEO-c, allowing for more precise measurements of these quantities.

There are two independent helicity amplitudes, the helicity-two amplitude ($\lambda = 2$) and the helicity-zero ($\lambda = 0$) amplitude, that contribute to $\chi_{c2} \rightarrow \gamma\gamma$ decay [5], where λ is the difference in the helicity values of the two photons. The ratio of the two-photon partial widths for the two helicity components, $f_{0/2} = \Gamma^{\lambda=0}_{\gamma\gamma}(\chi_{c2})/\Gamma^{\lambda=2}_{\gamma\gamma}(\chi_{c2})$ in the decay $\chi_{c2} \rightarrow \gamma\gamma$, is predicted to be about 0.5% [5]; a measurement of this ratio can be used to test the QCD prediction.

In this paper, $(1.06 \pm 0.04) \times 10^8$ ψ' events accumulated in BESIII are used to study the process $\psi' \rightarrow \gamma_1\chi_{c0,2}$, $\chi_{c0,2} \rightarrow \gamma_2\gamma_3$ and measure the two-photon decay widths, $\Gamma_{\gamma\gamma}(\chi_{c0})$ and $\Gamma_{\gamma\gamma}(\chi_{c2})$. We also determine the ratio $\mathcal{R}$, where many of the systematic uncertainties cancel in the ratio of the two simultaneous measurements. The ratio of the helicity-zero component relative to helicity-two component, $f_{0/2}$, is also reported for the first time.

II. THE BESIII EXPERIMENT AND DATA SET

This analysis is based on a 156.4 pb^{-1} of ψ' data corresponding to $(1.06 \pm 0.04) \times 10^8$ ψ' events [14] collected with the BESIII detector [15] operating at the BEPCII Collider [16]. In addition, an off-resonance sample

of 44.1 pb^{-1} taken at $\sqrt{s} = 3.65$ GeV is used for the study of continuum backgrounds.

BEPCII/BESIII [15] is a major upgrade of the BESII experiment at the BEPC accelerator [17] for studies of hadron spectroscopy and τ-charm physics [18]. The design peak luminosity of the double-ring e^+e^- collider, BEPCII, is 10^{33} cm^{-2} s^{-1} at a beam current of 0.93 A. The BESIII detector has a geometrical acceptance of 93% of 4π and consists of four main components: (1) a small-celled, helium-based main draft chamber with 43 layers. The average single wire resolution is 135 μm, and the momentum resolution for 1 GeV/c charged particles in a 1 T magnetic field is 0.5%; (2) an electromagnetic calorimeter (EMC) made of 6240 CsI (Tl) crystals arranged in a cylindrical shape (barrel) plus two end caps. For 1.0 GeV photons, the energy resolution is 2.5% in the barrel and 5% in the end caps, and the position resolution is 6 mm in the barrel and 9 mm in the end caps; (3) a time-of-flight system (TOF) for particle identification composed of a barrel part made of two layers with 88 pieces of 5 cm thick, 2.4 m long plastic scintillators in each layer, and two end caps with 96 fan-shaped, 5 cm thick, plastic scintillators in each end cap. The time resolution is 80 ps in the barrel, and 110 ps in the end caps, corresponding to a 2σ K/π separation for momenta up to about 1.0 GeV/c; (4) a muon chamber system made of 1000 m^2 of resistive plate chambers arranged in 9 layers in the barrel and 8 layers in the end caps and incorporated in the return iron of the superconducting magnet. The position resolution is about 2 cm.

The optimization of the event selection and the estimation of physics backgrounds are performed using Monte Carlo (MC) simulated data samples. The GEANT4-based simulation software BOOST [19] includes the geometric and material description of the BESIII detectors, the detector response and digitization models, as well as the tracking of the detector running conditions and performance. The production of the ψ' resonance is simulated by the Monte Carlo event generator KKMC [20]; the known decay modes are generated by EVTGEN [21] with branching ratios set at PDG [12] world average values, and by LUNDCHARM [22] for the remaining unknown decays. The analysis is performed in the framework of the BESIII offline software system [23] which takes care of the detector calibration, event reconstruction and data storage.

III. DATA ANALYSIS

Electromagnetic showers are reconstructed from clusters of energy deposits in the EMC crystals. The energy deposited in nearby TOF counters is included to improve the reconstruction efficiency and energy resolution. Showers identified as photon candidates are required to satisfy fiducial and shower-quality criteria. A photon candidate is a shower detected in the EMC with a total energy deposit greater than 25 MeV and with an angle θ with

respect to the e^+ beam direction in the range $|\cos\theta| <$ 0.75. This requirement is used to suppress continuum background $e^+e^- \to \gamma\gamma(\gamma)$, where the two energetic photons are mostly distributed in the forward and backward regions. We restrict the analysis to events that have no detected charged particles. The average event vertex of each run is assumed as the origin for the selected candidates. For $\psi' \to \gamma_1\chi_{c0,2}$, $\chi_{c0,2} \to \gamma_2\gamma_3$ analysis, events are required to have three photon candidates, among which the smallest energy photon is selected as the radiated photon γ_1 and the second-largest and the largest energy photons are defined as $\gamma_2\gamma_3$ from $\chi_{c0,2}$ decays. An energy-momentum conservation constraint 4C fit is performed, and events with $\chi^2 \leq 80$ are retained in the final selection. The energy spectrum of the radiated photons is shown in Fig. 1, where enhancements due to the χ_{c0} and χ_{c2} over substantial backgrounds are clearly observed.

To determine signal efficiencies 100 K signal MC event samples are generated for the χ_{c0} and the χ_{c2}, with PDG values for the masses and widths [12]. The radiative transition $\psi(2S) \to \gamma_1\chi_{c0}$ is generated using a $(1 + \cos^2\theta)$ distribution, where θ is the radiative photon angle relative to the positron beam direction, in accordance with expectations for pure $E1$ transitions. The $\chi_{c0} \to \gamma_2\gamma_3$ decays are generated using a uniform angular distribution. Although the radiative transition $\psi(2S) \to \gamma_1\chi_{c2}$ is dominantly pure $E1$ [24,25], there is some recent experimental evidence that the decay has contributions from higher-order multipoles [26]. The full angular amplitudes for $\psi' \to \gamma_1\chi_{c2}$ are discussed in association with Eq. (5) in Sec. 5. Furthermore, the $\gamma_2\gamma_3$ photons in the decay $\chi_{c2} \to \gamma_2\gamma_3$ are expected to be mostly in a pure helicity-two state; the ratio of the partial two-photon widths for the helicity-zero and helicity-two amplitudes is predicted to be less than 0.5% [5]. Thus the signal MC for the decay $\psi' \to \gamma_1\chi_{c2}$,
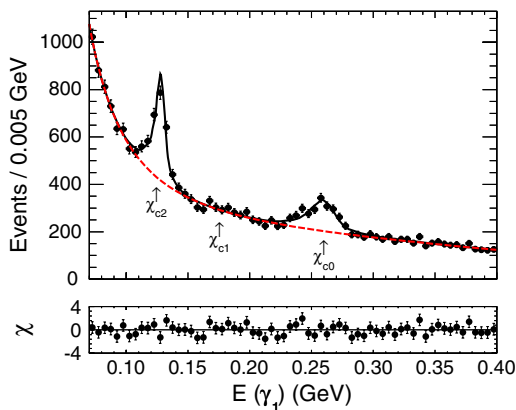

FIG. 1 (color online). Upper plot: The fitted E_{γ_1} spectrum for the ψ' data sample. The expected positions of E_{γ_1} from χ_{c0}, χ_{c1}, χ_{c2} are indicated by arrows. The dashed curve shows the background line shape fixed to the shape in Fig. 2. Lower plot: The number of standard deviations, χ, of data points from the fitted curves.

TABLE I. Expected numbers of background events peaking at the χ_{cJ} signal regions from MC simulations. The errors are the uncertainties from these measured branching fractions [14].

Decay modes	$n_{\chi_{c0}}$	$n_{\chi_{c2}}$
$\psi' \to \gamma\chi_{c0}$, $\chi_{c0} \to \pi^0\pi^0$	25.4 ± 2.2	0.0 ± 0.0
$\psi' \to \gamma\chi_{c0}$, $\chi_{c0} \to \eta\eta$	0.4 ± 0.1	0.0 ± 0.0
$\psi' \to \gamma\chi_{c2}$, $\chi_{c2} \to \pi^0\pi^0$	0.0 ± 0.0	7.7 ± 0.7
$\psi' \to \gamma\chi_{c2}$, $\chi_{c2} \to \eta\eta$	0.0 ± 0.0	0.1 ± 0.1
Sum	25.8 ± 2.2	7.8 ± 0.7

$\chi_{c2} \to \gamma_2\gamma_3$ is generated with $\gamma_2\gamma_3$ in a helicity-two state as described in Sec. 5.

The energy resolutions determined by the MC simulations are $\sigma(E_{\gamma_1}) = 6.74 \pm 0.29$ MeV for χ_{c0} and $\sigma(E_{\gamma_1}) = 3.91 \pm 0.09$ MeV for χ_{c2}. The efficiencies determined from MC simulations for the χ_{c0} and χ_{c2} are $\epsilon(\chi_{c0}) = (35.4 \pm 0.06)\%$ and $\epsilon(\chi_{c2}) = (38.0 \pm 0.07)\%$. The difference between $\epsilon(\chi_{c0})$ and $\epsilon(\chi_{c2})$ is due primarily to the different angular distributions.

The dominant nonpeaking background that is apparent in the spectrum in Fig. 1 is from continuum $e^+e^- \to \gamma\gamma(\gamma)$ processes. It is determined from MC simulations that contributions to the background due to radiative decays to the η, η', and 3γ decays of ψ' are nonpeaking, spread over the full range of E_{γ_1}, and negligible. Therefore, they do not change the shape of the dominant continuum background. In addition we use MC simulations to investigate possible sources of peaking backgrounds. These are found to come from $\chi_{c0,c2} \to \pi^0\pi^0$ and $\eta\eta$ decays and $\pi^0(\eta) \to \gamma\gamma$, where two of the γ's have low momentum and are not detected or are outside of the fiducial volume of this analysis. We generate at least 100 K events of each type to determine the efficiencies for the peaking backgrounds, and use the efficiencies and branching fractions measured by BESIII [14] to determine the numbers of peaking background events listed in Table I.

IV. MEASUREMENT OF BRANCHING FRACTIONS AND TWO-PHOTON WIDTHS

An unbinned maximum likelihood (ML) fit is done to the E_{γ_1} spectrum as shown in Fig. 1. The shape of the large nonpeaking background in the spectrum is determined with the 44.1 pb^{-1} of off-ψ' data taken at $\sqrt{s} = 3.65$ GeV, as well as the 921.8 pb^{-1} of $\psi(3770)$ data taken at $\sqrt{s} = 3.773$ GeV. As is evident in Fig. 2, the off-ψ' data are in good agreement with the high statistics $\psi(3770)$ data, for which transitions to either the χ_{c0} or χ_{c2} states are expected to be less than 8 events [12]. We also generate $e^+e^- \to \gamma\gamma(\gamma)$ MC events using the Babayaga QED event generator [27] and confirm that the shapes from the 3.65 and 3.773 GeV samples are consistent with being due to the QED process. The E_{γ_1} distribution for the $\psi(3770)$ data is fitted with the data-driven function:
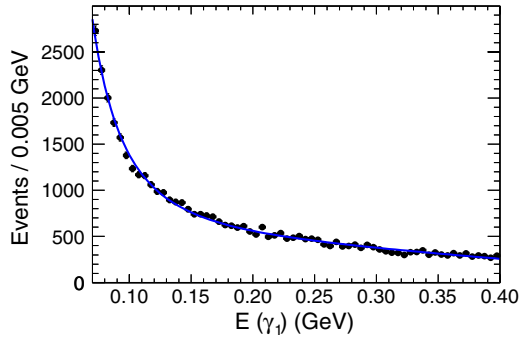
FIG. 2 (color online). The background E_{γ_1} spectrum. The points are from the off-ψ' data. The curve is from a fit to the $\psi(3770)$ data.
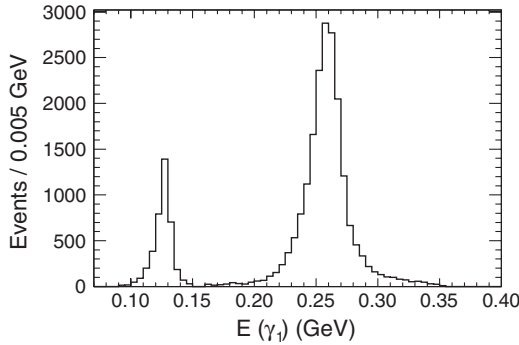

FIG. 3. The E_{γ_1} spectrum for the radiative photon in the samples $\psi' \to \gamma_1 \chi_{c0,2}$, $\chi_{c0,2} \to K^+ K^-$.

$$f_{bg}(E_{\gamma_1}) = p_0 + p_1 \times E_{\gamma_1} + p_2 \times (E_{\gamma_1})^a, \quad (2)$$

where p_0, p_1, p_2 and a are parameters which are obtained in a fit to the $\psi(3770)$ data in Fig. 2. In the nominal fit to the ψ' data, the background shape is fixed to Eq. (2), but its normalization is allowed to float. The shapes of the χ_{c0} and χ_{c2} resonances used in the fit are extracted from a nearly background-free $\psi' \to \gamma_1 \chi_{c0,2}$, $\chi_{c0,2} \to K^+ K^-$ sample shown in Fig. 3. The purity of the sample is larger than 99.2%. The shapes of the signal peaks in the $E\gamma_1$ spectrum are fixed to the smoothed histograms of the $\psi' \to \gamma_1 \chi_{c0,2}$, $\chi_{c0,2} \to K^+ K^-$ sample, and the yields are allowed to float.

The estimated numbers of peaking background events from $\chi_{c0,c2} \to \pi^0 \pi^0$ and $\eta\eta$ that contribute to the χ_{c0} and χ_{c2} signals are 25.8 and 7.8 events, respectively, as listed in Table I. They are subtracted from the fitted yields, and after this subtraction, the signal yields are $N(\chi_{c0}) = 813 \pm 63$ and $N(\chi_{c2}) = 1131 \pm 66$. The product branching fractions are determined from the relation

$$\mathcal{B}(\psi' \to \gamma \chi_{cJ}) \times \mathcal{B}(\chi_{cJ} \to \gamma\gamma) = \frac{N(\chi_{cJ})}{\epsilon(\chi_{cJ}) \times N_{\psi'}}, \quad (3)$$

where $N_{\psi'}$ is the total number of ψ' in the data sample. The measured product branching fractions are listed in Table II. We use the PDG average values,

$$\mathcal{B}(\psi' \to \gamma \chi_{c0}) = (9.68 \pm 0.31) \times 10^{-2},$$
$$\Gamma(\chi_{c0}) = (10.4 \pm 0.6) \text{ MeV},$$
$$\mathcal{B}(\psi' \to \gamma \chi_{c2}) = (8.75 \pm 0.35) \times 10^{-2},$$
$$\Gamma(\chi_{c2}) = (1.97 \pm 0.11) \text{ MeV}, \quad (4)$$

to determine $\mathcal{B}(\chi_{c0,2} \to \gamma\gamma)$, $\Gamma_{\gamma\gamma}(\chi_{c0,2})$ and $\mathcal{R}$. These are also listed in Table II.

Several sources of systematic uncertainties in the measurement of the branching fractions are considered, including uncertainties on the photon detection and reconstruction; the number of ψ' decays in the data sample; the kinematic fitting; the fitting procedure and peaking background subtraction. Table III lists a summary of all sources of systematic uncertainties. Most systematic uncertainties are determined from comparisons of special clean, high statistics samples with results from MC simulations.

The number of ψ' events, $N_{\psi'}$, used in this analysis is determined from the number of inclusive hadronic ψ' decays following the procedure described in detail in [14]. The result is $N_{\psi'} = (1.06 \pm 0.04) \times 10^8$, where the error is systematic.

Three photons in the final states include a soft photon γ_1 from the radiative transition and two energetic photons $\gamma_2 \gamma_3$ from $\chi_{c0,2}$ decays. The photon detection efficiency and its uncertainty for low energy photons are studied using three different methods described in Ref. [28]. On average, the efficiency difference between data and MC

TABLE II. Results of the present measurements. The first error is statistical, the second is systematic, and the third is due to the PDG values used. The common systematic errors have been removed in determining $\mathcal{R}$. $\mathcal{B}_1 \equiv \mathcal{B}(\psi' \to \gamma \chi_{c0,2})$, $\mathcal{B}_2 \equiv \mathcal{B}(\chi_{c0,2} \to \gamma\gamma)$, and $\Gamma_{\gamma\gamma} \equiv \Gamma_{\gamma\gamma}(\chi_{c0,2} \to \gamma\gamma)$.

Quantity	χ_{c0}	χ_{c2}
$\mathcal{B}_1 \times \mathcal{B}_2 \times 10^5$	$2.17 \pm 0.17 \pm 0.12$	$2.81 \pm 0.17 \pm 0.15$
$\mathcal{B}_2 \times 10^4$	$2.24 \pm 0.19 \pm 0.12 \pm 0.08$	$3.21 \pm 0.18 \pm 0.17 \pm 0.13$
$\Gamma_{\gamma\gamma}$ (keV)	$2.33 \pm 0.20 \pm 0.13 \pm 0.17$	$0.63 \pm 0.04 \pm 0.04 \pm 0.04$
$\mathcal{R}$		$0.271 \pm 0.029 \pm 0.013 \pm 0.027$

TABLE III. Summary of systematical uncertainties of the branching fraction measurements.

Source of systematic uncertainty	χ_{c0}	χ_{c2}
Number of ψ'[a]	4.0%	4.0%
Neutral trigger efficiency[a]	0.1%	0.1%
Photon detection[a]	1.5%	1.5%
Kinematic fit[a]	1.0%	1.0%
Resonance fitting	3.2%	2.9%
Peaking background	0.3%	0.1%
Helicity 2 assumption	$\cdots$	0.4%
Sum in quadrature	5.5%	5.3%

[a]The systematic sources common to both χ_{c0} and χ_{c2}.

simulation is less than 1% [28]. The momenta of the two energetic photons are more than 1.5 GeV/c. The systematic uncertainty due to the reconstruction of two energetic photons is determined to be 0.25% per photon as described in Ref. [29]. The total uncertainty associated with the reconstruction of the three photons is 1.5%.

The uncertainty due to the kinematic fit is estimated using a sample of $e^+e^- \rightarrow \gamma\gamma(\gamma)$, which has the same event topology as the signal. We select the sample by using off-ψ' data taken at $\sqrt{s} = 3.65$ GeV to determine the efficiency difference between data and MC for the requirement of $\chi^2_{4C} < 80$ in the 4C fit. The uncertainty due to kinematic fitting determined in this way is 1%.

Since the signal shapes are obtained from $\psi' \rightarrow \gamma\chi_{c0,2}$, $\chi_{c0,2} \rightarrow K^+K^-$ events in the data, the uncertainty due to the signal shape is negligible. The shape of the continuum background is parameterized using the data-driven function in Eq. (2); the parameters obtained in the fitting to off-ψ' data sample are fixed in the nominal fitting to ψ' data. The systematic uncertainty due to the choice of parametrization for the background shape is estimated by varying the fitting range and the order of polynomial in our data-driven function. We find relative changes on the χ_{c0}

and χ_{c2} signal yields of 3.2% and 2.9%, respectively, which are taken as the uncertainties due to the resonance fitting.

The expected numbers of peaking background events from $\chi_{c1,2} \rightarrow \pi^0\pi^0$ and $\chi_{c0,2} \rightarrow \eta\eta$ decays summarized in Table I use BESIII measurements for $\mathcal{B}(\chi_{c1,2} \rightarrow \pi^0\pi^0/\eta\eta)$ [14]. The uncertainties on the $\pi^0\pi^0/\eta\eta$ contributions are estimated to be 0.3% and 0.1% for χ_{c0} and χ_{c2}, respectively. The systematic uncertainties due to the trigger efficiency in these neutral channels are estimated to be $<0.1\%$, based on cross-checks using different trigger conditions [14,30]. We have assumed pure helicity-two decay of $\chi_{c2} \rightarrow \gamma\gamma$. In a relativistic calculation, Barnes [5] predicted the helicity-zero component to be 0.5%. In Sec. 5, the ratio of the two photon widths for the helicity-zero and helicity-two amplitudes is measured to be $0.00 \pm 0.02 \pm 0.02$. To be conservative, we determine the change in our χ_{c2} result when a helicity-zero component of 3% is included, corresponding to an upper limit at 90% confidence level from the measurement in this paper, to be 0.4%, and use that as the helicity-state-associated systematic error.

All sources of systematic errors are listed in Table III. We assume that all systematical uncertainties are independent and add them in quadrature to obtain the total systematical uncertainty. For the measurements of $\mathcal{B}(\chi_{c0,2} \rightarrow \gamma\gamma)$, the uncertainty due to the $\psi' \rightarrow \gamma\chi_{c0,2}$ branching fractions is kept separate and quoted as a second systematic uncertainty.

V. HELICITY AMPLITUDE ANALYSIS FOR $\chi_{c2} \rightarrow \gamma\gamma$

In $\chi_{c2} \rightarrow \gamma\gamma$ decay, the final state is a superposition of helicity-zero ($\lambda = 0$) and helicity-two ($\lambda = 2$) components, where λ is the difference in the helicity values of the two photons. The formulas for the helicity amplitudes in $\psi' \rightarrow \gamma\chi_{c2}, \chi_{c2} \rightarrow \gamma\gamma$, which include higher-order multipole amplitudes, are

$$
\begin{aligned}
W_2(\theta_1, \theta_2, \phi_2) = f_{0/2} \bigg[&\frac{3}{2}y^2(1 + \cos^2\theta_1)\sin^4\theta_2 + 3x^2\sin^2\theta_1\sin^2 2\theta_2 - \frac{3\sqrt{2}}{2}xy\sin 2\theta_1\sin^2\theta_2\sin 2\theta_2\cos\phi_2 \\
&+ \sqrt{3}x\sin 2\theta_1\sin 2\theta_2(3\cos^2\theta_2 - 1)\cos\phi_2 + \sqrt{6}y\sin^2\theta_1\sin^2\theta_2(3\cos^2\theta_2 - 1)\cos 2\phi_2 \\
&+ (1 + \cos^2\theta_1)(3\cos^2\theta_2 - 1)^2 \bigg]_{\lambda=0} \\
&+ \bigg[\frac{1}{4}y^2(1 + \cos^2\theta_1)(1 + 6\cos^2\theta_2 + \cos^4\theta_2) + 2x^2\sin^2\theta_1(1 + \cos^2\theta_2)\sin^2\theta_2 \\
&+ \frac{\sqrt{2}}{4}xy\sin 2\theta_1\sin 2\theta_2(3 + \cos^2\theta_2)\cos\phi_2 - \frac{\sqrt{3}}{2}x\sin 2\theta_1\sin^2\theta_2\sin 2\theta_2\cos\phi_2 \\
&+ \frac{\sqrt{6}}{2}y\sin^2\theta_1(1 - \cos^4\theta_2)\cos 2\phi_2 + \frac{3}{2}(1 + \cos^2\theta_1)\sin^4\theta_2 \bigg]_{\lambda=2},
\end{aligned}
\tag{5}
$$

where $x = A_1/A_0$, $y = A_2/A_0$, and $A_{0,1,2}$ are the χ_{c2} helicity 0, 1, 2 amplitudes, respectively, θ_1 is the polar angle of the radiative photon, where the electron beam is defined as the z axis in the e^+e^- center-of-mass frame, and θ_2 and ϕ_2 are the polar angle and azimuthal angle of one of the photons from χ_{c2} decay in the χ_{c2} rest frame, relative to the radiative photon direction as polar axis; $\phi_2 = 0$ is defined by the electron beam direction. The factor $f_{0/2} = |F_0|^2/|F_2|^2 = \Gamma_{\gamma\gamma}^{\lambda=0}(\chi_{c2})/\Gamma_{\gamma\gamma}^{\lambda=2}(\chi_{c2})$ is the ratio of partial two-photon widths for the helicity-zero and helicity-two components, where F_0 (F_2) is the helicity-zero (two) amplitude in the decay $\chi_{c2} \rightarrow \gamma\gamma$. Further information on the formulas for the helicity amplitudes can be found in Ref. [31].

An unbinned ML fit to the angular distribution is performed to determine x, y and $f_{0/2}$ values. We define 12 factors [26]:

$$a_1 = 3\sin^2\theta_1\sin^2 2\theta_2, \tag{6}$$

$$a_2 = \tfrac{3}{2}(1 + \cos^2\theta_1)\sin^4\theta_2, \tag{7}$$

$$a_3 = -\frac{3\sqrt{2}}{2}\sin2\theta_1\sin^2\theta_2\sin2\theta_2\cos\phi_2, \tag{8}$$

$$a_4 = \sqrt{3}\sin2\theta_1\sin2\theta_2(3\cos^2\theta_2 - 1)\cos\phi_2, \tag{9}$$

$$a_5 = \sqrt{6}\sin^2\theta_1\sin^2\theta_2(3\cos^2\theta_2 - 1)\cos2\phi_2, \tag{10}$$

$$a_6 = (1 + \cos^2\theta_1)(3\cos^2\theta_2 - 1)^2, \tag{11}$$

$$a_7 = 2\sin^2\theta_1(1 + \cos^2\theta_2)\sin^2\theta_2, \tag{12}$$

$$a_8 = \tfrac{1}{4}(1 + \cos^2\theta_1)(1 + 6\cos^2\theta_2 + \cos^4\theta_2), \tag{13}$$

$$a_9 = \frac{\sqrt{2}}{4}\sin2\theta_1\sin2\theta_2(3 + \cos^2\theta_2)\cos\phi_2, \tag{14}$$

$$a_{10} = -\frac{\sqrt{3}}{2}\sin2\theta_1\sin^2\theta_2\sin2\theta_2\cos\phi_2, \tag{15}$$

$$a_{11} = \frac{\sqrt{6}}{2}\sin^2\theta_1(1 - \cos^4\theta_2)\cos2\phi_2, \tag{16}$$

$$a_{12} = \tfrac{3}{2}(1 + \cos^2\theta_1)\sin^4\theta_2. \tag{17}$$

The mean values of $a_1, \ldots, a_{12}$ can be determined with $\psi' \rightarrow \gamma\chi_{c2}$, $\chi_{c2} \rightarrow \gamma\gamma$ MC events, where phase space is used for the simulation of all the angular distributions:

$$\bar{a}_n = \frac{\sum_{i=1}^N a_n(i)}{N}, n = 1, \ldots, 12, \tag{18}$$

where N is the number of events after all selections from phase space MC samples. Since $\bar{a}_n$ is calculated with phase space MC events after selection, it naturally accounts for the detector acceptance effects.

The normalized probability-density function is written as

$$f(x, y, f_{0/2}) = \frac{W_2(\theta_1, \theta_2, \phi_2|x, y, f_{0/2})}{f_{0/2}(\bar{a}_1 x^2 + \bar{a}_2 y^2 + \bar{a}_3 xy + \bar{a}_4 x + \bar{a}_5 y + \bar{a}_6) + (\bar{a}_7 x^2 + \bar{a}_8 y^2 + \bar{a}_9 xy + \bar{a}_{10} x + \bar{a}_{11} y + \bar{a}_{12})}. \tag{19}$$

A total log-likelihood function is constructed as $\ln\mathcal{L} = \sum_{i=1}^n \ln f_i(x, y, f_{0/2})$, where the sum is over all the events in the signal region (here the signal region is defined as $0.09 < E_{\gamma_1} < 0.15$ GeV). The log-likelihood function for the signal is given by $\ln\mathcal{L}_s = \ln\mathcal{L} - \ln\mathcal{L}_b$, in which $\ln\mathcal{L}_b$ is the normalized sum of logarithmic likelihood values from background events and is calculated using the events in the sidebands, which are defined in the ranges (0.07, 0.08) GeV (lower sideband) and (0.16, 0.20) GeV (higher sideband) in the E_{γ_1} spectrum. By maximizing the logarithm of the likelihood function $\ln\mathcal{L}_s$, the best values of x, y and $f_{0/2}$ are determined. Before fitting to the data, input and output checks were done using MC samples, and the results used to validate the fitting procedure.

BESIII has determined x and y to be $x = 1.55 \pm 0.05(\text{stat}) \pm 0.07(\text{syst})$ and $y = 2.10 \pm (\text{stat})0.07 \pm 0.05(\text{syst})$ [26] using the decays $\psi' \rightarrow \gamma\chi_{c2}$, $\chi_{c2} \rightarrow \pi^+\pi^-/K^+K^-$. Therefore, in the nominal fit, the x and y parameters are fixed to the measured values, and the remaining parameter $f_{0/2}$ is determined to be

$$f_{0/2} = 0.00 \pm 0.02, \tag{20}$$

where the error is statistical. Figure 4 shows the angular distributions of background-subtracted data and the fitted results for $\chi_{c2} \rightarrow \gamma\gamma$ events. It is found that all angular distributions are consistent with the fitted results within errors. As mentioned in Sec. 4, for the measurements of the branching fractions we use the formulas in Eq. (5) to generate MC events for efficiency determination of $\psi' \rightarrow \gamma\chi_{c2}$, $\chi_{c2} \rightarrow \gamma\gamma$ decay, with the x, y and $f_{0/2}$ parameters fixed at their measured central values ($x = 1.55$, $y = 2.10$ and $f_{0/2} = 0.0$).

In order to test the reliability of the fit, we allow the x and y parameters to float in the fit, in which case the likelihood fit to data yields
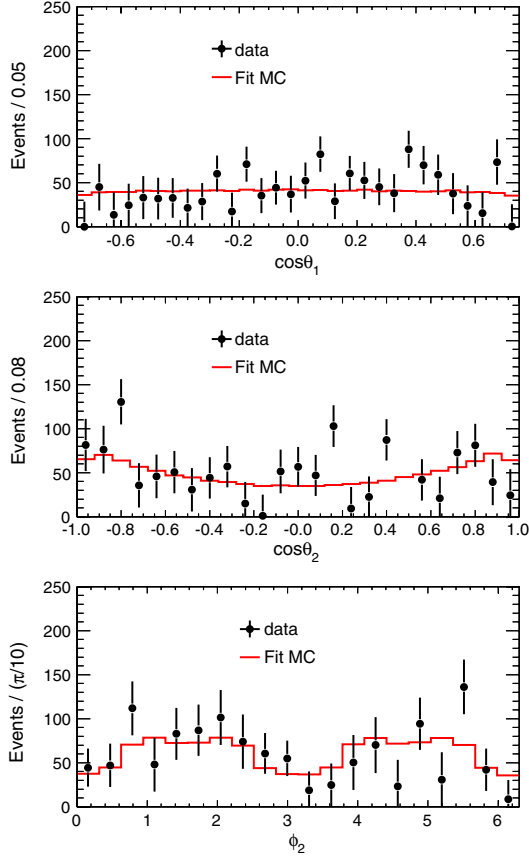
FIG. 4 (color online). Distributions of $\cos\theta_1$, $\cos\theta_2$ and ϕ_2 for the $\psi' \to \gamma\chi_{c2}$, $\chi_{c2} \to \gamma\gamma$, where the dots with error bars are background-subtracted data and the histograms are the fitted results.

$$x = 1.76 \pm 0.25, \qquad y = 2.00 \pm 0.23, \qquad (21)$$

where the errors are statistical. The results are consistent with the previous BESIII measurements of the $\psi' \to \gamma\chi_{c2}$, $\chi_{c2} \to \pi^+\pi^-/K^+K^-$ decays [26].

The goodness of the fit is estimated using Pearson's χ^2 test [32]. The data and MC are divided into 6 bins of equal

width in each dimension (i.e. $\cos\theta_1$, $\cos\theta_2$, ϕ_2) of the three-dimension angular distribution. The numbers of events in each cell for data and the normalized MC sample are compared. The χ^2 is defined as

$$\chi^2 = \sum_i \frac{(n_i^{DT} - n_i^{MC})^2}{\sigma_{n_i^{DT}}^2}, \qquad (22)$$

where n_i^{DT} ($\sigma_{n_i^{DT}}$) is the observed number (its error) of signal events after background subtraction in the ith bin from data and n_i^{MC} is the expected number of events predicted from MC in the ith bin using $f_{0/2}$ fixed to the value determined in the analysis. If the number of events in a bin is less than 5, we add the events to the adjacent bin. The result of the χ^2 test of the fitting is $\chi^2/\text{ndf} = 87.3/88 = 0.99$, where ndf is the number of degrees of freedom. The result shows that the fit quality is acceptable.

Since $f_{0/2}$ is a ratio, many systematic errors cancel, and only the effects due to MC simulation of detector response, the uncertainties on the measured x and y parameters, background substraction, χ_{c0} contamination are considered here. Among these sources of the systematic uncertainties, the MC simulation of detector response is dominant; the others are tiny and are neglected.

As discussed above, the x and y parameters are fixed to the measured values from Ref. [26] in the ML fit to $\chi_{c2} \to \gamma\gamma$ events in order to obtain the ratio $f_{0/2}$. In the fit we change the x and y central values by 1 standard deviation of the measured values [26], and find that the effect on $f_{0/2}$ is negligible. To estimate the uncertainty due to background subtraction, we vary the sideband region from (0.07, 0.08) GeV (lower sideband) and (0.16, 0.20) GeV (higher sideband) to (0.07, 0.09) GeV and (0.15, 0.20) GeV. After subtraction of the background based on the sum of recalculated logarithmic likelihood values, $\ln\mathcal{L}_b$, we find that the fitted $f_{0/2}$ value is almost unchanged. From MC simulation, 0.028% of the $\chi_{c0} \to \gamma\gamma$ events are distributed under the χ_{c2} signal region; the

TABLE IV. The comparison of experimental results for the two-photon partial widths of χ_{c0} and χ_{c2}.

Quantity	PDG global fit results[a]	CLEO-c[b]	This measurement[b]
$\mathcal{B}_1 \times \mathcal{B}_2 \times 10^5 (\chi_{c0})$[c]	2.16 ± 0.18	$2.17 \pm 0.32 \pm 0.10$	$2.17 \pm 0.17 \pm 0.12$
$\mathcal{B}_1 \times \mathcal{B}_2 \times 10^5 (\chi_{c2})$[c]	2.24 ± 0.17	$2.68 \pm 0.28 \pm 0.15$	$2.81 \pm 0.17 \pm 0.15$
$\mathcal{B}_2 \times 10^4 (\chi_{c0})$[c]	2.23 ± 0.17	$2.31 \pm 0.34 \pm 0.15$	$2.24 \pm 0.19 \pm 0.15$
$\mathcal{B}_2 \times 10^4 (\chi_{c2})$[c]	2.56 ± 0.16	$3.23 \pm 0.34 \pm 0.24$	$3.21 \pm 0.18 \pm 0.22$
$\Gamma_{\gamma\gamma}(\chi_{c0})$ (keV)	2.32 ± 0.22	$2.36 \pm 0.35 \pm 0.22$	$2.33 \pm 0.20 \pm 0.22$
$\Gamma_{\gamma\gamma}(\chi_{c2})$ (keV)	0.50 ± 0.05	$0.66 \pm 0.07 \pm 0.06$	$0.63 \pm 0.04 \pm 0.06$
$\mathcal{R}$	0.22 ± 0.03	$0.28 \pm 0.05 \pm 0.04$	$0.27 \pm 0.03 \pm 0.03$
$f_{0/2}$	$\cdots$	$\cdots$	$0.00 \pm 0.02 \pm 0.02$

[a]The results from the literature have been reevaluated by using the branching fractions and total widths from the PDG global fit.
[b]The first error is statistical. The second error is a systematic error combined in quadrature with the error in the branching fractions and widths used.
[c]$\mathcal{B}_1 \equiv \mathcal{B}(\psi(2s) \to \gamma\chi_{c0,c2})$, $\mathcal{B}_2 \equiv \mathcal{B}(\chi_{c0,c2 \to \gamma\gamma})$, and $\Gamma_{\gamma\gamma}(\chi_{c0,c2}) \equiv \Gamma_{\gamma\gamma}(\chi_{c0,c2 \to \gamma\gamma})$.

uncertainty due to χ_{c0} contamination is estimated to be negligible.

The uncertainty due to the inconsistency between data and MC simulation on the angular distributions for χ_{c2} events can be tested using χ_{c0} events. Since the χ_{c0} is pure helicity zero, the x and y parameters are expected to be zero. In $\chi_{c0} \rightarrow \gamma\gamma$ decay, the difference of helicity values of the two photons is also expected to be zero, so only the helicity-zero term in Eq. (5) remains, which modifies Eq. (5) to

$$
\begin{aligned}
W_0(\theta_1, \theta_2, \phi_2) = &\left[\frac{3}{2}y^2(1 + \cos^2\theta_1)\sin^4\theta_2 + 3x^2\sin^2\theta_1\sin^2 2\theta_2 - \frac{3\sqrt{2}}{2}xy\sin 2\theta_1\sin^2\theta_2\sin 2\theta_2\cos\phi_2 \right.\\
&+ \sqrt{3}x\sin 2\theta_1\sin 2\theta_2\cos\phi_2 + \sqrt{6}y\sin^2\theta_1\sin^2\theta_2\cos 2\phi_2 + (1 + \cos^2\theta_1) \Big]_{\lambda=0}\\
&+ f_{2/0}\left[\frac{1}{4}y^2(1 + \cos^2\theta_1)(1 + 6\cos^2\theta_2 + \cos^4\theta_2) + 2x^2\sin^2\theta_1(1 + \cos^2\theta_2)\sin^2\theta_2 \right.\\
&+ \frac{\sqrt{2}}{4}xy\sin 2\theta_1\sin 2\theta_2(3 + \cos^2\theta_2)\cos\phi_2 - \frac{\sqrt{3}}{2}x\sin 2\theta_1\sin^2\theta_2\sin 2\theta_2\cos\phi_2\\
&+ \frac{\sqrt{6}}{2}y\sin^2\theta_1(1 - \cos^4\theta_2)\cos 2\phi_2 + \frac{3}{2}(1 + \cos^2\theta_1)\sin^4\theta_2 \Big]_{\lambda=2},
\end{aligned}
\tag{23}
$$

where the product factor $f_{0/2}$ is moved to the front factor of the helicity-two term and renamed as $f_{2/0}$, and the $(3\cos^2\theta_2 - 1)^2$ term associated with $\lambda = 0$ amplitude in Eq. (5) is replaced by 1, so that one can obtain the expected angular distribution $W_0 = 1 + \cos^2\theta_1$ from Eq. (23) if the parameters $x = 0$, $y = 0$ and $f_{2/0} = 0$, as expected. Therefore, we fit the angular distribution of χ_{c0} with the Eq. (23) using the same method as in χ_{c2} decays; nonzero x, y and $f_{2/0}$ values will indicate the inconsistency between data and MC simulation. The systematic error is taken as the shift from 0 plus its error. The fitted results are $x = -0.11 \pm 0.09$, $y = 0.13 \pm 0.07$ and $f_{2/0} = 0.00 \pm 0.02$. The correlation coefficient between x and y is -0.27, while it is 0.0 between x (y) and $f_{2/0}$. Thus we take 0.02 as the systematic error for the measurement of $f_{0/2}$ in the fit to χ_{c2} events. Studies with MC simulated data samples demonstrate that a systematic error in modeling the θ_1, θ_2, and ϕ_2 efficiency produces a shift of approximately the same size for $f_{2/0}$ in χ_{c0} sample and $f_{0/2}$ in χ_{c2} sample, when the latter sample is generated with $x = 1.55$, $y = 2.10$ and $f_{0/2} = 0$. Therefore, we assume the observed shift from $f_{2/0}$ for the true χ_{c0} data is an estimate of the systematic error on the measured values of $f_{0/2}$ for the two-photon decay of χ_{c2}.

VI. CONCLUSION

In summary, we present measurements of the two-photon decays of $\chi_{c0,2}$ via the radiative decays $\psi' \rightarrow \gamma\chi_{c0,2}$. We find $\mathcal{B}(\chi_{c0} \rightarrow \gamma\gamma) = (2.24 \pm 0.19 \pm 0.15) \times 10^{-4}$ and $\mathcal{B}(\chi_{c2} \rightarrow \gamma\gamma) = (3.21 \pm 0.18 \pm 0.22) \times 10^{-4}$, which agree with the results from the CLEO experiment [13]. The partial widths $\Gamma_{\gamma\gamma}(\chi_{c0,c2})$ and the ratio $\mathcal{R}$ of the two-photon partial widths between χ_{c2} and χ_{c0} are determined from these measurements. The precision of our measurements is improved compared to CLEO's; the final results are listed in Table IV.

Since theoretical unknowns cancel in the ratio $\mathcal{R}$, a calculation including the first-order radiative corrections by Voloshin [33] predicts $\mathcal{R}_{\text{th}}^{(1)} = 0.116 \pm 0.010$. Our experimental result, $\mathcal{R} = 0.27 \pm 0.04$, indicates some inadequacy of the first-order radiative corrections that have been used to make theoretical predictions for charmonium decays.

We also perform a helicity amplitude analysis for the decay of $\psi' \rightarrow \gamma\chi_{c2}$, $\chi_{c2} \rightarrow \gamma\gamma$; the ratio of the two-photon partial widths for the helicity-zero and helicity-two components in the decay $\chi_{c2} \rightarrow \gamma\gamma$ is determined for the first time to be $f_{0/2} = 0.00 \pm 0.02 \pm 0.02$. The helicity-zero component in the $\chi_{c2} \rightarrow \gamma\gamma$ decay is highly suppressed. This measurement is consistent with the calculations based on a relativistic potential model [5], in which the ratio is predicted to be less than 0.5%.

---

[1] H. W. Huang, C. F. Qiao, and K. T. Chao, Phys. Rev. D **54**, 2123 (1996); C. W. Hwang and R. S. Guo, Phys. Rev. D **82**, 034021 (2010).

[2] R. Barbier, R. Gatto, and R. Kögerler, Phys. Lett. **60B**, 183 (1976).

[3] L. Laudau, Phys. Abstr. A **52**, 125 (1949); C. N. Yang, Phys. Rev. **77**, 242 (1950).

[4] T. Appelquist and H. D. Politzer, Phys. Rev. Lett. **34**, 43 (1975).

[5] T. Barnes, in *Proceedings of the IX International Workshop on Photon-Photon Collisions* edited by D. O. Caldwell and H. P. Paar (World Scientific, Singapore, 1992), p. 263.

[6] S. N. Gupta, J. M. Johnson, and W. W. Repko, Phys. Rev. D **54**, 2075 (1996).

[7] D. Ebert, R. N. Faustov, and V. O. Galkin, Mod. Phys. Lett. A **18**, 601 (2003); Phys. Rev. D **67**, 014027 (2003).

[8] S. Godfrey and N. Isgur, Phys. Rev. D **32**, 189 (1985).

[9] G. A. Schuler, F. A. Berends, and R. van Gulik, Nucl. Phys. **B523**, 423 (1998).

[10] J. P. Lansberg and T. N. Pham, Phys. Rev. D **79**, 094016 (2009).

[11] J. J. Dudek and R. G. Edwards, Phys. Rev. Lett. **97**, 172001 (2006).

[12] K. Nakamura *et al.* (Particle Data Group), J. Phys. G **37**, 075021 (2010), and 2011 partial update for the 2012 edition.

[13] K. M. Ecklund *et al.* (CLEO Collaboration), Phys. Rev. D **78**, 091501(R) (2008).

[14] M. Ablikim *et al.* (BES Collaboration), Phys. Rev. D **81**, 052005 (2010).

[15] M. Ablikim *et al.* (BES Collaboration), Nucl. Instrum. Methods Phys. Res., Sect. A **614**, 345 (2010).

[16] J. Z. Bai *et al.* (BES Collaboration), Nucl. Instrum. Methods Phys. Res., Sect. A **344**, 319 (1994); **627**, 319 (2001).

[17] J. Z. Bai *et al.* (BES Collaboration), Nucl. Instrum. Methods Phys. Res., Sect. A **344**, 319 (1994); **458**, 627 (2001).

[18] Special issue on Physics at BESIII, edited by K. T. Chao and Y. F. Wang [Int. J. Mod. Phys. A **24**, 3, Supp. (2009)].

[19] S. Agostinelli *et al.* (GEANT4 Collaboration), Nucl. Instrum. Methods Phys. Res., Sect. A **506**, 250 (2003).

[20] S. Jadach, B. F. L. Ward, and Z. Was, Comput. Phys. Commun. **130**, 260 (2000); Phys. Rev. D **63**, 113009 (2001).

[21] D. J. Lange, Nucl. Instrum. Methods Phys. Res., Sect. A **462**, 152 (2001).

[22] J. C. Chen, G. S. Huang, X. R. Qi, D. H. Zhang, and Y. S. Zhu, Phys. Rev. D **62**, 034003 (2000).

[23] W. D. Li *et al.*, in *Proceedings of CHEP06, Mumbai, India, 2006* edited by Sunanda Banerjee (Tata Institute of Fundamental Research, Mumbai, 2006).

[24] M. Oreglia *et al.* (Crystal Ball Collaboration), Phys. Rev. D **25**, 2259 (1982).

[25] M. Ambrogiani *et al.* (E835 Collaboration), Phys. Rev. D **65**, 052002 (2002).

[26] M. Ablikim *et al.* (BES Collaboration), Phys. Rev. D **84**, 092006 (2011).

[27] C. M. Carloni Calame, G. Montagna, O. Nicrosini, and F. Piccinini, Nucl. Phys. B, Proc. Suppl. **131**, 48 (2004), and references therein.

[28] M. Ablikim *et al.* (BES Collaboration), Phys. Rev. D **83**, 112005 (2011).

[29] M. Ablikim *et al.* (BES Collaboration), Phys. Rev. Lett. **105**, 261801 (2010).

[30] N. Berger, K. Zhu, Z.-A. Liu, D.-P. Jin, H. Xu, W.-X. Gong, K. Wang, and G.-F. Cao, Chinese Phys. C **34**, 1779 (2010).

[31] T. Luo, G. Li, H. B. Li, and Z. H. Yu, "The deduction of the angular distribution of $\chi_{c2} \rightarrow \gamma\gamma$" (unpublished).

[32] W. Eadie *et al.*, *Statistical Methods in Experimental Physics* (North-Holland Publishing Company, Amsterdam-London, 1971).

[33] M. B. Voloshin, Prog. Part. Nucl. Phys. **61**, 455 (2008).